The Evolution of the Lymanα Forest

Jan Peter Mücket[1], Patrick Petitjean[2,3], Rüdiger Riediger[1]

[1] *Astrophysikalisches Institut Potsdam*
An der Sternwarte 16, D–14482 Potsdam, Germany
[2] *Institut d'Astrophysique de Paris, CNRS*
98bis Boulevard Arago, F–75014 Paris, France
[3] *UA CNRS 173- DAEC, Observatoire de Paris-Meudon,*
Principal Cedex, F–92195 Meudon, France

1 Introduction

Over the past half decade considerable progress has been made in the theoretical understanding of the nature of the Lymanα forest. The common outcome of related investigations (Cen et al. 1994, Petitjean et al. 1995, Mücket et al. 1996, Hernquist et al. 1996, Miralda-Escudé et al. 1996, Zhang et al. 1996, Bi & Davidsen 1996) is the interpretation of the Lymanα absorption as originated by an inhomogeneous IGM pervaded by a background ionizing radiation field. The latter is probably originated by QSOs and/or star-forming galaxies. In all recent models a direct relation between the Lymanα forest and the cosmological structure formation is presumed. Since the results obtained from the simulations agree with the corresponding quantities from observation already quantitatively it could be expected that further investigations could lead to new constraints with respect to the underlying cosmological models. Since observational data are available now at almost all redshifts up to z=5 one would wish to model the complete lines of sight in order to link the Lymanα forest evolution at high and low redshifts. The hydro-simulations are already able to give a very detailed description of the Lymanα forest. The amount of computing time is such however that most of the descriptions are limited to $z > 2$. Using assumptions that have been shown to be valid in the low density regime we study the evolution of the Lymanα forest over the whole redshift range $5 > z > 0$.

2 Simulations

Our assumption that the Lymanα gas traces the shallower potential wells of the dark matter distribution, i.e. Ω_b is assumed to be constant all the time, allows for using numerical simulations including collisionless particles only. Thus the needed computational time can be decreased considerably. This approximation has been shown to be valid for the low-density regime characteristic of the Lymanα forest by detailed hydro-simulations (see Miralda-Escudé et al. 1996, Hernquist et al. 1996, Yepes et al. 1997, and also Gnedin et al. 1997, Hui et al. 1997). A procedure to determine the gas temperature assuming that energy is acquired by the gas when shell-crossing takes place in the dark matter dynamics has been introduced according to Kates et al. (1991).

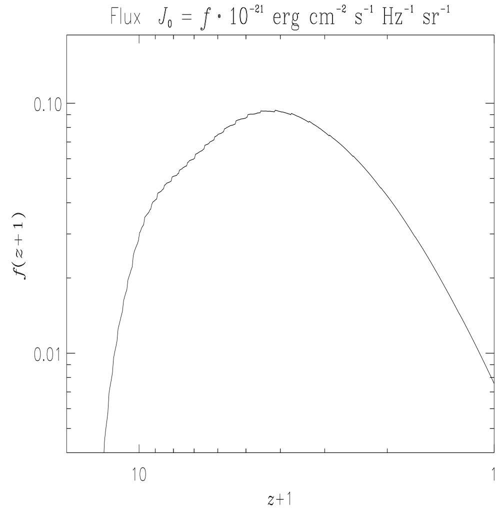

Figure 1: Evolution of the UV-background intensity from the simulation

Once the gas associated with the particles has been assigned a temperature the subsequent thermal history is followed as described in Mücket et al. (1996) taking into account adiabatic effects, radiative cooling processes, Compton cooling and heating by photo-ionization. The gas content of particles not undergoing shell-crossing is assumed to be in thermal equilibrium given by cooling and heating processes. The simulations use 128^3 particles on a 256^3 grid and were carried out using a box size of 12.8 Mpc, which corresponds to a co-moving cell size of 50 kpc. We adopt a value for the Hubble parameter $H_0 = 50$ km Mpc^{-1} s^{-1} and $\Omega_{\mathrm{b}} = 0.05$ throughout.

The intensity of the photo-ionizing UV background flux, assumed to be homogeneous and isotropic inside the simulation box, is computed in the course of the simulation. The ionizing spectrum is modeled as $J_\nu \propto J_0\,\nu^{-1}$ where $J_0 = f(z) = J_{-21} \cdot 10^{-21}$ erg cm^{-2} s^{-1} Hz^{-1} sr^{-1} is the ionizing flux at 13.6 eV. The variation of the flux intensity with redshift z is related both to the rate $\Delta m(T_4 < 0.5; z)$ at which the baryonic material cools below $T_4 = 0.5$ (with $T = T_4 \cdot 10^4$ K) in the simulation and to the expansion of the Universe. We further assume that the cool gas is transformed into stars with an efficiency ε of about 8%. The remainder of the gas is reheated to temperatures above 50 000 K. The characteristic time scale for such processes is of order $t_* \approx 10^8$ years. We distinguish between particles for which shock heating is important enough to significantly increase the gas temperature above the temperature resulting from photo-ionization (population $P_{\rm s}$) and the remainder of the particles (population $P_{\rm u}$). Population $P_{\rm s}$ particles are mostly found in big halos and elongated filamentary structures (regions of enhanced density). The population $P_{\rm u}$ is present in the surroundings of the structures formed by shocked particles but mostly in the voids delineated by these structures. The fraction of particles belonging to population $P_{\rm u}$ is changing with time: 77% at z=3, 67% at z=2, 40% at z=0.5 and 25% at z=0.

3 Results

We use the simulation to synthesize spectra along a line of sight to a fictitious QSO at $z = 5$ (s. also Riediger et al., this volume). A first test of the model is that the evolution of the average Lymanα decrement should be reproduced. The evolution with redshift of the ionizing flux is computed assuming that its variation is related to the amount of gas that collapses in the simulation at any time. The only free parameter is the normalization of $J_{-21}(z)$. A value

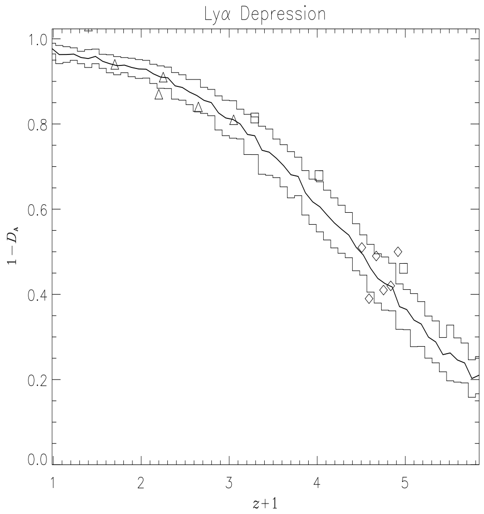

Figure 2: Lymanα decrement versus redshift. Observed data are from: diamonds, Lu et al. (1996); triangles, a compilation by Jenkins & Ostriker (1991) at low redshifts; squares: Rauch et al. (1997)

of $J_{-21}(z_0) = 0.1$ at $z_0 \sim 3$ (see Fig. 1) fits the decrement evolution quite well (see Fig. 2). Compared with constraints obtained for the flux intensity from observations at various redshifts (s. e.g. Haardt & Madau 1996) this value may appear as too low. A discussion of possible reasons for that discrepancy is given in Riediger et al. (1997).

An important quantity to be compared with observations is the number density per unit redshift interval and its time-dependent behavior. It can be seen from Fig. 3 that the evolution of the total number of strong lines is well reproduced. Data are taken from Lu et al. (1991), Petitjean et al. (1993) and Bahcall et al. (1993). If the number of lines per unit redshift is approximated by a power-law, $\mathrm{d}n/\mathrm{d}z \propto (1+z)^{\gamma}$, we find $\gamma \approx 2.6$ for $1.5 < z < 3$ and $\gamma \approx 0.6$ for $0 < z < 1.5$(after smoothing). However the slope of dn/dz steepens at $z > 3$. Fitting the number density evolution for $1.5 < z < 5$ by a single power law we get $\gamma \approx 2.9$. Fig. 4 shows the contributions of the two populations of

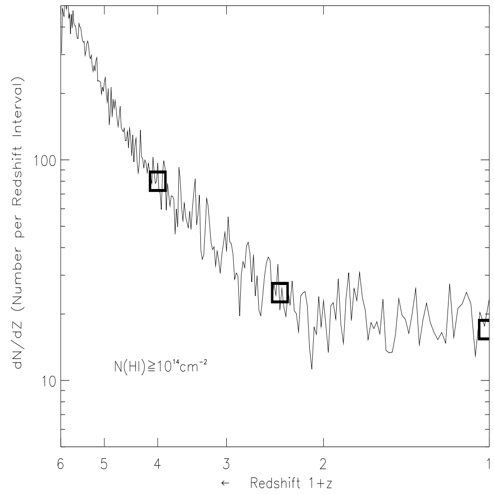

Figure 3: Number density $\mathrm{d}n/\mathrm{d}z$ of clouds with column density $\log N(\mathrm{H\,I}) > 14$ versus redshift z

clouds with $N(\mathrm{H\,I}) > 10^{14}$ cm^{-2}, P_{s} (solid line) and P_{u} (dash-dotted line). It is apparent that the dominant population is different before and after $z \sim 3$. At high redshift, most of the lines arise in P_{u} particles whereas at low redshift, most of the gas is condensed in filamentary structures (see Petitjean et al. 1995). The very steep slope found for the number density evolution of the P_{u} clouds as shown in Fig. 4 is mainly due to decreasing H I column densities through individual clouds.

The number density of lines with $N(\mathrm{H\,I}) > 10^{12}$ cm^{-2} is about constant over the redshift range $1 < z < 5$ (see Fig. 5) and decreases slowly at lower redshift. Note, however that due to the limited resolution the number density at $z > 3$ for column densities $N(\mathrm{H\,I}) < 10^{12.5}$ cm^{-2} is probably underestimated. Low density gas is found in regions delineated by filamentary structures at high redshift. This gas slowly disappears. The total number density of lines stays nearly constant because the high column density gas has column density decreasing with time. This difference in the evolution of the number

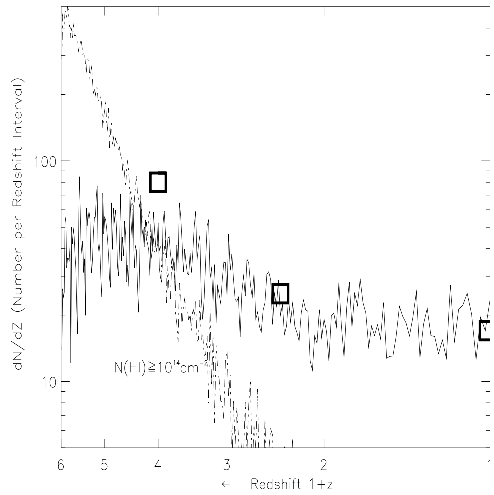

Figure 4: As Fig. 3. The number density of lines drawn from populations $P_{\rm s}$ and $P_{\rm u}$ are plotted as full and dash-dotted lines respectively

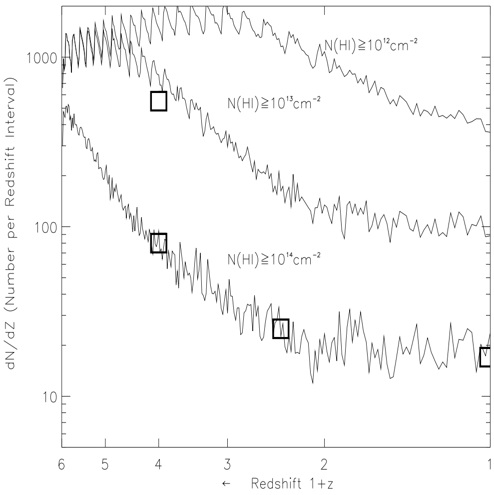

Figure 5: Number density of lines versus redshift for different column densities thresholds $\log N(\rm H\,I) > 12, 13, 14$

density of weak and strong lines has been noticed in intermediate resolution data (Bechtold 1994) and confirmed by Kim et al. (1997). The latter authors find $\gamma = 2.41 \pm 0.18$ and 1.29 ± 0.45 for $\log N(\rm H\,I) > 10^{14}$ and10^{13} cm^{-2}

respectively.

The resulting column density distribution (cp. Fig. 2 shown in Riediger et al., this volume) as well as the distribution of Doppler parameters determined from the simulated spectra show a remarkable agreement with the observations. On the basis of these results it appears encouraging enough to make predictions for redshifts at $z \sim 0$:

The number density of lines per unit redshift at $z \sim 0$ with column densities $\log N(\mathrm{H\,I}) > 12, 13, 14$ is expected to be 400, 100, and 20 respectively. At low redshift, if most of the strong ($w_{\mathrm{r}} > 0.3$ Å) lines are associated with galaxies, the bulk of the Lymanα forest however should have lower equivalent width and should not be tightly correlated with galaxies. Our model predicts that the number of weak lines should be large at low redshift and gives therefore an interesting test of the overall picture. This prediction can be tested along the line of sight to 3C273 with the new instrumentation on the Hubble Space Telescope.

References

[1] Bahcall J.N., Bergeron J., Boksenberg A., et al.; *ApJS 87*, 1993, 1

[2] Bechtold J., 1994, *ApJ* S 91, 1

[3] Cen R., Miralda-Escudé J., Ostriker J.P., Rauch M., 1994, *ApJL* 437, L9

[4] Gnedin Y.N., Hui L., 1997, astro-ph/9706219

[5] Haardt F., Madau P., 1996, *ApJ* 461, 20

[6] Hernquist L., Katz N., Weinberg D.H.,et al., 1996, *ApJ* 457, L51

[7] Hu E.M., Kim T.-S., Cowie L.L., Songaila A., Rauch M.; *AJ 110*, 1995, 1526

[8] Hui L., Gnedin N.Y., Zhang Y., 1997, astro-ph/9702167

[9] Lu L., Wolfe A.M., Turnshek D.A.; *ApJ 367*, 1991, 19

[10] Kates R.E., Kotok E.V., Klypin A.A., 1991, *A&A* 243, 295

[11] Kim T.-S., Hu E.M., Cowe L.L., Songaila A., 1997, astro-ph/9704184

[12] Miralda-Escudeé J., Cen R., Ostriker J.P., Rauch M., 1996, *ApJ* 471, 582

[13] Morris S.L., Weymann R.J., Savage B.D., et al., 1991, *ApJL* 377, 21

[14] Mücket J.P., Petitjean P., Kates R., Riediger R.; *A&A 308*, 1996, 17

[15] Petitjean P., Webb J.K., Rauch M., et al.; *MNRAS 262*, 1993, 499

[16] Petitjean P., Mücket J., Kates R.E., 1995, *A&A* 295, L9

[17] Riediger R., Petitjean P., Mücket J.P.; *A&A*, 1997, accepted

[18] Tripp T., et al., 1997, preprint

[19] Yepes G., Kates R., Khokhlov A., Klypin A., 1997, *MNRAS* 284, 235

[20] Zhang Y., Meiksin A., Anninos P., Norman M.L.; astro-ph/9609194